Influence of coil contact on static behavior of helical compression springs

F De Crescenzo[1] **and P Salvini**[1]
[1] University of Rome “Tor Vergata", Department of Enterprise Engineering
Via del Politecnico,1 00133 Rome Italy
francesco.de.crescenzo@uniroma2.it

Abstract. Large deformations of helical springs are affected by coil contact, but most available spring modelling techniques only account for nonlinear vertical motion, and Finite Elements (FE) nonlinear analysis that considers contact between coils can be very expensive. A 2D model based on equivalent beam and penalty-based contact algorithm is developed for efficient yet realistic prediction of non-uniform spring deflection. The proposed model is tested versus FE, where the helical wire is modelled using beam elements. Two scenarios are taken into account: a cylindrical spring in compression/bending and a progressive conical spring under simple compression. It is shown that the proposed model matches FE at a very low computational cost.

1. Introduction

In many applications, contact between coils of helical compression springs allows introducing extra damping and increasing stiffness in the system while deforming. Just to give an example, this has been widely used for valve springs in internal combustion engines over the last decades [1]. Simulation of such systems, where nonlinear springs are involved, requires an appropriate modelling strategy. A full simulation of the coiled wire, e.g. using finite elements, would be too expensive to run and a correct managing of contact algorithm is nontrivial. Therefore, most commercial packages provide several tools to account for the nonlinear springs at a lower computational cost. A common approach is the multi mass model, where the spring is represented by several masses connected with a sequence of stiffness and damping elements [2]. Usually the parameters are computed from coils properties, and nonlinearity arises as the gaps between consecutive masses close. It is also possible to directly provide the nonlinear spring characteristics, obtained from previous computations (analytically or via finite elements) or direct experiments. However, these methods only account for vertical motion and it seems to the authors that there is a lack in literature about the influence of coils contact on flexural and lateral behavior. In these cases, clash between coils not only affect the stiffness, but also changes the direction of spring motion and the volume occupied during operation.

Starting from Haringx’s work on instability [3], several researchers have studied the lateral motion of compression springs. Analytical solutions have been obtained using equivalent beams under large displacements, [4] [5], but these models cannot manage coils contact. On the other end, the dynamics of the wire has been addressed by many authors using numerical methods: finite elements [6] , transfer matrix method [7], finite differences [8], dynamic stiffness matrix method [9]. However, also in those cases it is still hard, and in some cases not practicable, to account for coil contacts and large deflection. In this paper a modelling strategy for nonlinear spring with coil contact is presented, with the aim of providing a tool for quick and accurate prediction of the component behavior. The proposed model takes advantage of the equivalent beam formulation and discretizes the spring with nonlinear beam-like

elements placed along the axis of the helix. At the same time, contact surfaces are related to the nodes and it is possible to introduce contact relations between adjacent coils. By this way, the contact acts in its real geometric occurrence and can provide both axial and radial effects, within the limits due to the in-plane formulation. The equivalent beam formulation is based on the assumptions of nonlinear Haringx's model and is discussed in section 2. Then, the contact definition is described in sections 3. Finally, several numeric examples are provided, considering FE as benchmark and conclusions are drawn.

2. 2D equivalent beam discrete model

2.1 Outline of the model

An illustration of the model is given in Figure 1. The spring is represented by beam elements (green) along helix axis, representing half a coil. Each node is associated with a contact zone (white) located where the working plane intersect the coiled wire. The 3D render of the spring can be obtained from nodal displacements and rotations.

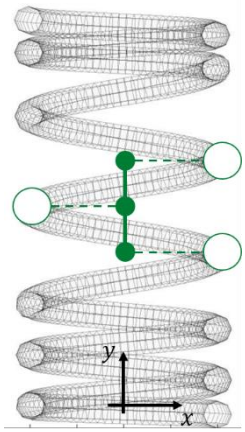

Figure 1. 2D equivalent beam model of a spring.

2.2 Large displacement kinematics and internal forces

Haringx studied the buckling of springs referring to beams following the spring axis [3]. Although, otherwise from classical Timoshenko beam [10], Haringx's equivalent beam rotation is only affected by the bending component. This implies that compression and shear reactions are oriented according to the rotation of cross-section due to bending. In the following, normal and shear directions are oriented according to Haringx's assumption: an illustration is given in Figure 2.

Elastic forces are assumed to be linear function of elongation, shear displacement, and cross-section rotation:

$$N = K_{ax}(l - l_0) \tag{1}$$

$$T = K_{sh}(v - v_0) \tag{2}$$

$$M = K_{fl}(\Delta\theta - \Delta\theta_0) \tag{3}$$

Where the subscript 0 refers to the undeformed configuration (usually $v_0 = 0$ and $\Delta\theta_0 = 0$). K_{ax} K_{sh} K_{fl} are axial, bending and shearing stiffness of half a coil, computed according to Haringx's hypothesis. For a wire with constant circular cross section with diameter *d*, and coil diameter *D*, they are:

$$K_{ax} = 2\frac{Gd^4}{8D^3}\cos p$$

$$K_{sh} = 2\frac{Ed^4}{8D^3}\cos p$$

$$K_{fl} = 2\frac{4EGd^4}{64D(2G+E)}\cos p$$

where p is helix angle, G and E are elastic and torsion modulus of the material. Average properties of half a coil are taken in case of non-uniform springs.

The factor $\cos p$ is omitted by Haringx, but it is here introduced, as in [2], to account for the effect of the helix angle on the real wire length, while the effect of helix angle on wire bending and torsional moments is neglected. Indeed, when considering the stress state in the wire, it is costume to neglect the helix angle due to the consideration that bending and torsion add themselves in the wire [11].

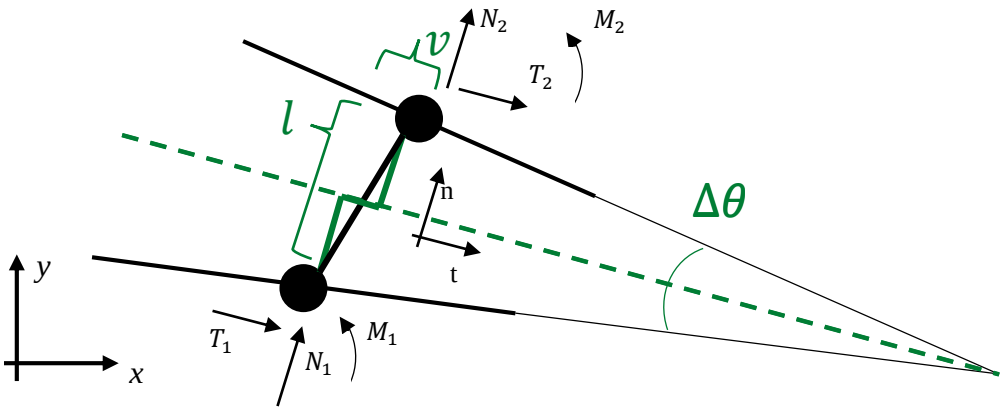

Figure 2. Half-coil element.

Equilibrium equations in local coordinate system of the element write:

$$N_1 + N_2 = 0 \tag{4}$$

$$T_1 + T_2 = 0 \tag{5}$$

$$M_1 + M_2 + N_2 v - T_2 l = 0 \tag{6}$$

Together with equations (1), (2), (3) they give:

$$N_2 - N_1 = K_{ax}(l - l_0) \tag{7}$$

$$T_2 = -T_1 = K_{sh}(v - v_0) \tag{8}$$

Assuming that bending reaction is equal to the average of the moments applied at the nodes it follows that:

$$\frac{M_2 - M_1}{2} = K_{fl}(\Delta\theta - \Delta\theta_0)$$

And from rotational equilibrium:

$$M_2 = 2K_{fl}(\Delta\theta - \Delta\theta_0) + M_1 = K_{fl}(\Delta\theta - \Delta\theta_0) - N_2\frac{v}{2} + T_2\frac{l}{2} \quad (9)$$

In global cartesian coordinate system, the half-coil element has six degrees of freedom. The corresponding generalized coordinates and forces are:

$$\boldsymbol{p} = \{x_1, y_1, \theta_1, x_2, y_2, \theta_2\}$$

$$\boldsymbol{F} = \left\{F_{x_1}, F_{y_1}, M_1 F_{x_2}, F_{y_2}, M_2\right\}$$

Only rotations $\Delta\theta$ can be directly computed, while l and v, nonlinearly depend on $\boldsymbol{p}$ components.

Tangent and normal to the cross section are oriented, respectively:

$$\boldsymbol{t} = \begin{pmatrix}\cos\theta_b \\ \sin\theta_b\end{pmatrix}$$

$$\boldsymbol{n} = \begin{pmatrix}-\sin\theta_b \\ \cos\theta_b\end{pmatrix}$$

where θ_b is the average angle orienting the equivalent beam element:

$$\theta_b = \frac{(\theta_2 + \theta_1)}{2}$$

Deformed length and shear displacement are then:

$$l = \boldsymbol{a} \cdot \boldsymbol{n}$$

$$v = \boldsymbol{a} \cdot \boldsymbol{t}$$

Where $\boldsymbol{a}$ is the vector connecting the nodes:

$$\boldsymbol{a} = \begin{pmatrix}x_2 - x_1 \\ y_2 - y_1\end{pmatrix}$$

Given l and v, internal forces are computed using equations (7), (8), (9) and as a matter of fact, the kinematics of the system gives the resulting internal forces.

2.3Stiffness matrix

Stiffness matrix should be derived from internal forces and displacements. However, for this study it was preferred to use the matrix of the analytical shearing beam, where cross section and material properties are substituted by axial, shearing and bending stiffness. The element matrix than writes:

$$K = \begin{bmatrix} K_{ax} & 0 & 0 & -K_{ax} & 0 & 0 \\ 0 & \frac{12K_{fl}}{L^2(1+\Phi)} & \frac{6K_{fl}}{L(1+\Phi)} & 0 & \frac{-12K_{fl}}{L^2(1+\Phi)} & \frac{6K_{fl}}{L(1+\Phi)} \\ & & \frac{K_{fl}(4+\Phi)}{(1+\Phi)} & 0 & \frac{-6K_{fl}}{L(1+\Phi)} & \frac{K_{fl}(2-\Phi)}{(1+\Phi)} \\ & & & K_{ax} & 0 & 0 \\ & Sym & & & \frac{12K_{fl}}{L^2(1+\Phi)} & \frac{-6K_{fl}}{L(1+\Phi)} \\ & & & & & \frac{K_{fl}(4+\Phi)}{(1+\Phi)} \end{bmatrix}$$

Where shearing factor Φ can be computed as:

$$\Phi = \frac{K_{fl}}{K_{sh}L^2}$$

3. Contact implementation

3.1 Contact kinematics and force

A penalty-based contact algorithm has been developed to account for coils contact in a realistic, yet efficient manner. The contact is evaluated on working plane using contact circles A and B in figure 3. Those circles are obtained as the intersection of the working plane with the spring wire (neglecting a secondary effect due to helix angle). When the distance between centers is less than the mean wire diameter, a contact force generates. The direction of the force is that of the line connecting the center of the two circles. Of course, the forces are applied to nodes 1 and 3 involved in contact and thus a moment arise. Thus, the contact is computed in the real location where it develops and then transferred to the equivalent beam nodes.

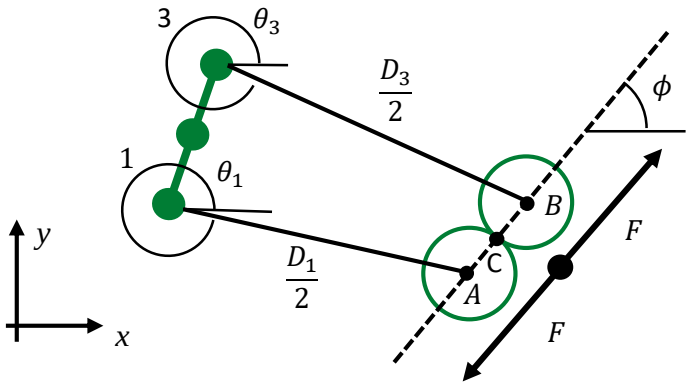

Figure 3. Contact description.

With reference to figure 3, the coordinates of contact circles centers are:

$$\begin{Bmatrix} x_A \\ y_A \end{Bmatrix} = \begin{Bmatrix} x_1 \\ y_1 \end{Bmatrix} + \frac{D_1}{2}\begin{Bmatrix} \cos\theta_1 \\ \sin\theta_1 \end{Bmatrix} \tag{10}$$

$$\begin{Bmatrix} x_B \\ y_B \end{Bmatrix} = \begin{Bmatrix} x_3 \\ y_3 \end{Bmatrix} + \frac{D_3}{2}\begin{Bmatrix} \cos\theta_3 \\ \sin\theta_3 \end{Bmatrix} \tag{11}$$

Thus, it is possible to compute the actual distance and penetration:

$$h = \sqrt{(x_A - x_B)^2 + (y_A - y_B)^2}$$

$$\overline{d} = \frac{1}{2}(d_1 + d_3)$$

Introducing a convenient contact force expression [2] with appropriate stiffness and exponent:

$$\begin{cases} F = K_C(\overline{d} - h)^k \\ (\overline{d} - h) > 0 \end{cases} \tag{12}$$

Angle ϕ gives the direction of the force and allows to calculate the coordinates of contact point C:

$$\cos\phi = \frac{x_B - x_A}{h}$$

$$\sin\phi = \frac{y_B - y_A}{h}$$

$$\begin{Bmatrix} x_C \\ y_C \end{Bmatrix} = \begin{Bmatrix} x_A - \frac{d_3}{2}\cos\phi \\ y_A - \frac{d_3}{2}\sin\phi \end{Bmatrix} = \begin{Bmatrix} x_B + \frac{d_1}{2}\cos\phi \\ y_B + \frac{d_1}{2}\sin\phi \end{Bmatrix} \tag{13}$$

Combining equations (10) and (13), and magnitude F from equation (12), it is possible to compute the generalized nodal forces, as function of nodal coordinates only:

$$\boldsymbol{F_1} = \begin{Bmatrix} F_{1x} \\ F_{1y} \\ M_1 \end{Bmatrix} = F \begin{Bmatrix} -\cos\phi \\ -\sin\phi \\ \sin\phi\,(\frac{D_1}{2}\cos\theta_1 + \frac{d_1}{2}\cos\phi) - \cos\phi\,(\frac{D_1}{2}\sin\theta_1 + \frac{d_1}{2}\sin\phi) \end{Bmatrix}$$

$$\boldsymbol{F_2} = \begin{Bmatrix} F_{3x} \\ F_{3y} \\ M_3 \end{Bmatrix} = F \begin{Bmatrix} \cos\phi \\ \sin\phi \\ \sin\phi\,(\frac{D_3}{2}\cos\theta_3 - \frac{d_3}{2}\cos\phi) - \cos\phi\,(\frac{D_3}{2}\sin\theta_2 - \frac{d_3}{2}\sin\phi) \end{Bmatrix}$$

3.2 Contact stiffness matrix

Contact stiffness matrix is given by contact forces derivatives with respect to nodal degrees of freedom. The expression is trivial but tedious and is easily computed using symbolic solver. The first column is obtained as follows:

$$K_{11} = \frac{\partial F_{x1}}{\partial x_1}, \qquad K_{21} = \frac{\partial F_{y1}}{\partial x_1}, \qquad K_{31} = \frac{\partial M_1}{\partial x_1}, \qquad K_{41} = \frac{\partial F_{x3}}{\partial x_1}, \qquad K_{51} = \frac{\partial F_{y3}}{\partial x_1}, \qquad K_{61} = \frac{\partial M_3}{\partial x_1}$$

4. Numerical examples

The model is tested versus FE simulation, for two different geometries and loads. The first example, Spring A, is a cylindrical spring with uniform pitch, clamped at bottom coil. The top coil is loaded by a force with both axial and lateral components. The second example, Spring B, is a conical spring loaded

axially and top coil is laterally constrained, to prevent buckling. Properties of the springs are listed in table 1. Direction of the force is constant (the force is not following coil rotation).

Design and modeling of end turns is not straightforward, in this work every spring ends with a full non-active turn, whose pitch is equal to the wire diameter (closed coil end). The FE model of the spring consists of beam elements, modeling the wire. The ending turns are pseudo-rigid regions, where all the nodes are connected to a central node using beam elements of higher stiffness. Bottom central node is fixed, while top central node can only move in the X-Y plane. For spring 2 it was necessary to activate the no-sliding option to help convergence of the finite element solution. Details of finite element modeling of the springs are listed in table 2.

Figure 4 shows undeformed Spring A (wireframe) and deformed configurations from both proposed model (blue) and FE (red) results. The two shapes are practically superimposed and is hard to distinguish between them. Load deflections curves at loaded node are plotted in figure 5. It is possible to notice the effect of contacts, especially on the vertical displacement of the tip. Furthermore, it is noticed that the proposed model is always showing a softer behavior than FE, in both with and without contact solutions.

Deformation of Spring B at maximum load is shown in figure 6 and the load-displacement characteristic of the spring in figure 7. Again, it is hard to distinguish between the rendering based on the proposed model and that based on finite elements.

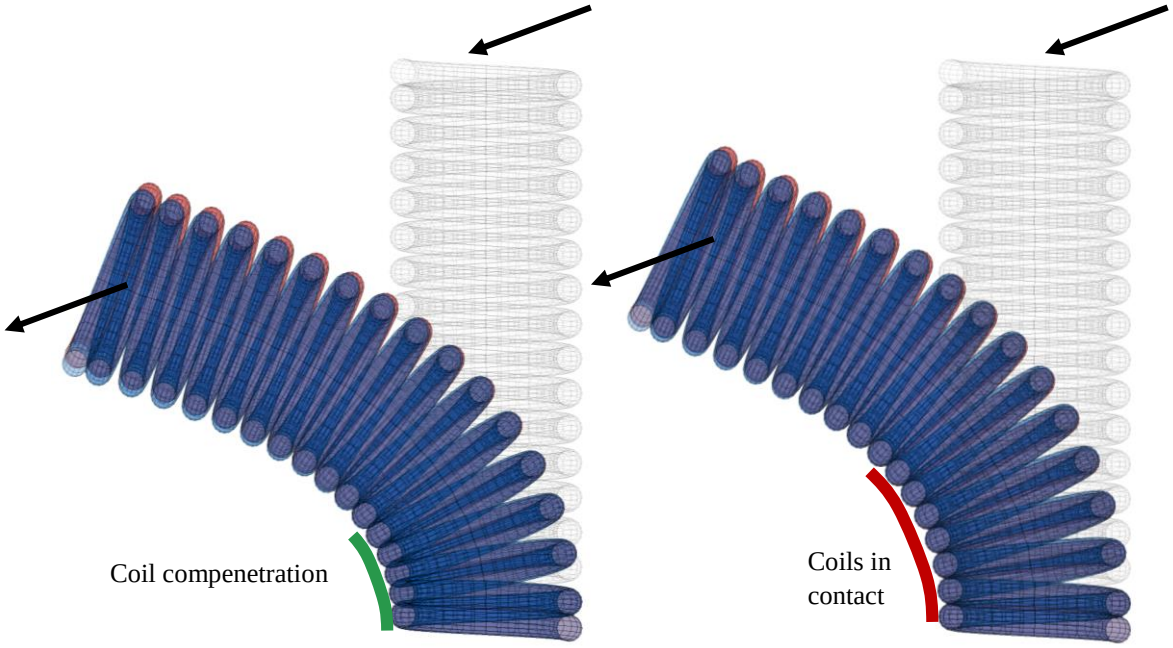

Figure 4. Spring A deformed at maximum load, without coil contact (left) and with coil contact. Proposed model result is blue and FE is red.

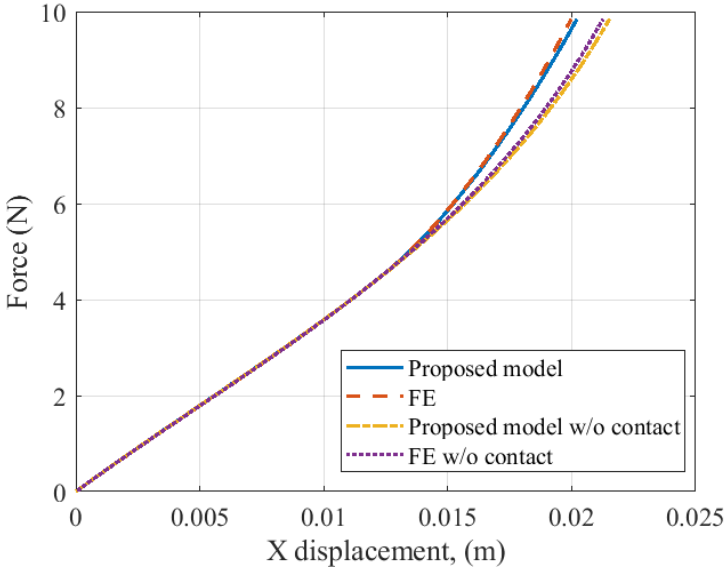

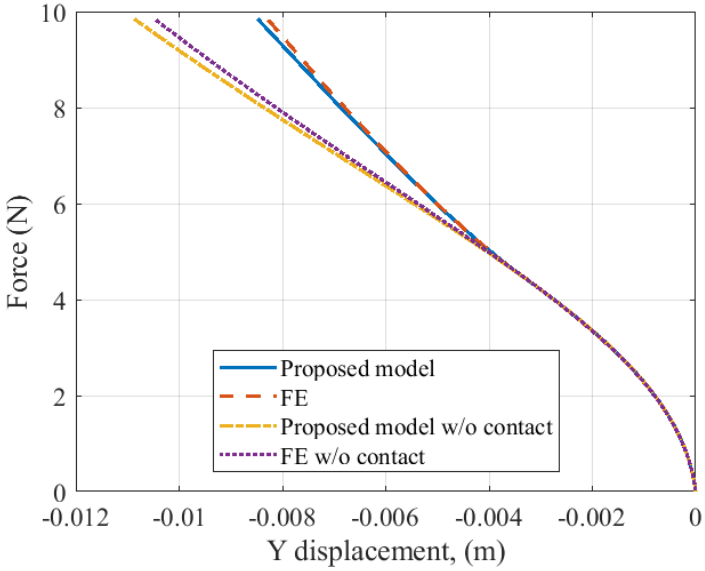

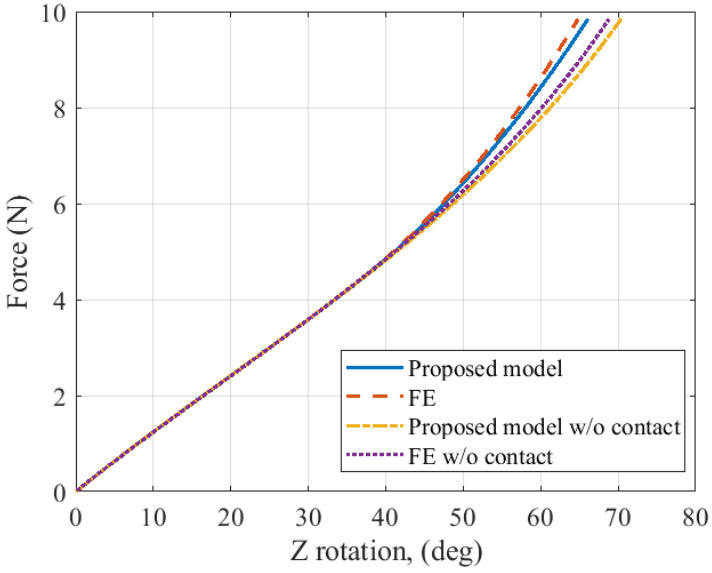

Figure 5. Spring A, displacements at tip.

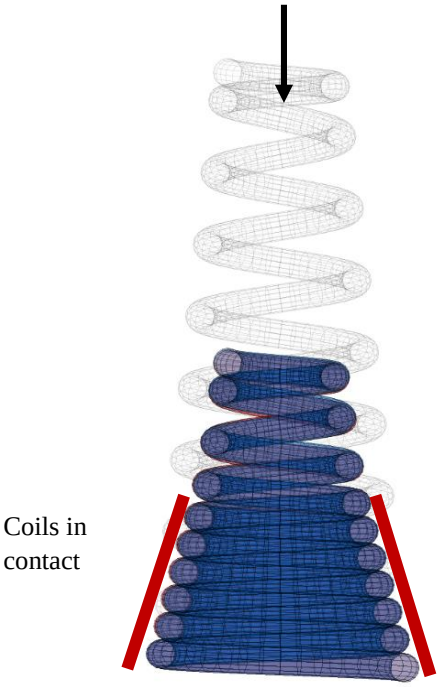

Figure 6. Spring B deformed configuration at maximum load. Result of proposed model in blue, FE in red.

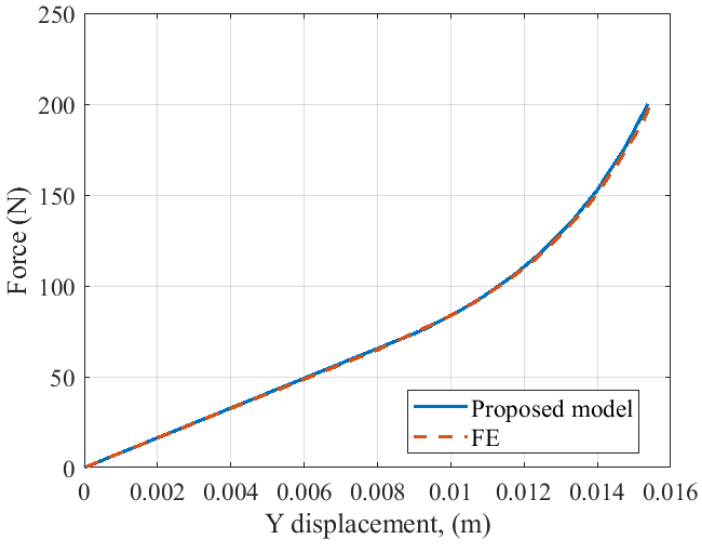

Figure 7. Load-deflection characteristic of spring B, proposed model (solid) and FE (dashed).

Table 1. Properties of the springs used in the examples.

Feature	Spring A	Spring B
Wire diameter (mm)	1.5	1.5
Mean bottom coil diameter (mm)	10	12
Mean top coil diameter (mm)	10	6
Number of active coils	14.5	7.5
Number of non-active coils	2	2
Pitch of non-active coils (mm)	1.5	1.5
Active height of spring (mm)	28.6	28.6
Total height of spring (mm)	31.6	31.6
Fx at time 1 (N)	-9	0
Fy at time 1 (N)	-4	-200

Table 2. Finite elements model of the springs.

Element type	2D Beam
Number of elements per turn	40
Contact element	Sphere to sphere contact (no sliding for spring 2)
Number contact elements per turn	4
Bottom node constrained dofs	ALL
Top node constrained dofs	UZ, ROTX, ROTY, (also UX, ROTZ, for spring 2)

Table 3. Solution time for proposed model and FE simulations.

Case	Finite elements (s)	Proposed model (s)	Reduction
Spring A	154	24	84%
Spring A w/o contacts	81	38	53%
Spring B	122	8	93%
Spring B w/o contacts	68	4	94%

A further interesting point is the comparison of the computer time to obtain the solution between the FE and the proposed model. In table 3 the comparison is done keeping the same step size in the nonlinear solution and it appears that, when contact affects the solution, the proposed model is much more competitive.

It is also possible to make some considerations about the impact of contact on computing time. It seems that contact is little affecting the solution time for FE simulation of Spring A, while it is even helping convergence for the proposed model. The behavior of the proposed model can be explained with the consideration that coil contact is preventing very large deformation of bottom coils, which in the non-contact case are compenetrating.

On the other hand, the presence of contact almost doubles the solution time of Spring B for both modeling techniques, but in this case, the non-contact scenario is absolutely unrealistic, since the spring telescopes with the top coil going under the bottom. Finally, it is interesting to notice that the proposed model shows a great difference in solution time between the two cases Spring A and Spring B. Figure 8 shows the number of iterations required at each substep when contact is considered. In fact, Spring B, excluding contact, is linear (only compression and no geometric effects) and before first contact occurs,

converges at first iteration. Conversely, nonlinear geometric effects are dominating large displacements in Spring A and an increasing number of iterations are required as the solution proceeds.

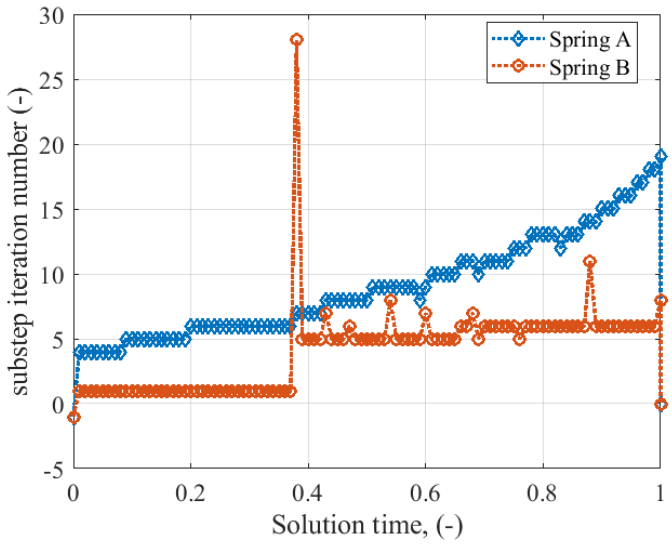

Figure 8. Proposed model substep iterations.

4. Conclusions

The provided examples show that the proposed model matches static finite elements simulations, even though a quite simple nonlinear model has been assumed for the half-coil deformation. Indeed, nonlinear phenomena like radial expansion and changing of helix angle due to deformation are neglected but may be implemented in the future.

Another important limit of the proposed model is the assumption of in-plane motion. This is a quite complex aspect that involves the effect of ending turns, which is hard to account also in FEM analysis. However, developing at least a 3D equivalent beam, with quarter-coil elements, is just a matter of implementation.

Finally, it seems important to remark that the proposed model took less than 1/6 of the time of the FEM for spring A and about 1/20 for spring B, when running on the same machine. Since there is still room for improvement in the algorithm, the proposed 2D nonlinear static model is thought to be an interesting basis for addressing more complex dynamic problems.

Bibliography

[1] Blair G P, McCartan C and Cahoon W 2010 Measurement and Computation of the Characteristics of - Progressive Valve Springs *SAE International* 2010-01-1056

[2] Schamel A, Hammacher J and Utsch D 1993 Modeling and Measurement Techniques for Valve Spring Dynamics in High Revving Internal Combustion Engines *SAE Technical Paper 930615*

[3] Haringx J A 1948 On highly compressible helical springs and rubber rods, and their application fo vibration-free mountings, part I *Philips Research Reports* vol 3 (Eindhoven: Philps research Laboratories) pp 401-49

[4] Mizuno M 1960 Problem of large deflection of coiled springs, *Bulletin of JSME* **3** 95-103

[5] Michalczyk K 2015 Analysis of lateral Vibrations of the Axially Loaded Helical Spring *J. Theor. App. Mech-Pol* **53** 745-55

[6] Mottershead J E 1982 The large displacements and dynamic stability of springs using helical finite elements *Int. J. Mech. Sci.* **24** 547-58

[7] Becker L E, Chassie G G and Cleghorn W L 2001 On the natural frequencies of helical compression springs *Int. J. Mech. Sci.* **44** 825-41

[8] Lin Y Y and Pisano A P 1990 Three-dimensional dynamic simulation of helical compression springs *J Mech Des* **112** 529-37

[9] Lee J and Thompson D J 2001 Dynamic stiffness formulation, free vibration and wave motion of helical springs *J Sound Vib* **239** 297-320

[10] Timoshenko S P and Gere J M 1985 *Theory of elastic stability*, (New York: McGraw-Hill Book)

[11] Wahl A 1963 *Mechanical Springs* (New York: McGraw-Hill Book)